Self-similarity of the plasma edge fluctuations

B. A. Carreras
Oak Ridge National Laboratory, Oak Ridge, Tennessee 37831-8070

B. Ph. van Milligen, M. A. Pedrosa, R. Balbín, and C. Hidalgo
Asociacíon Euratom-Ciemat, 28040 Madrid, Spain

D. E. Newman
Oak Ridge National Laboratory, Oak Ridge, Tennessee 37831-8070

E. Sánchez, M. Frances, and I. García-Cortés
Asociacíon Euratom-Ciemat, 28040 Madrid, Spain

J. Bleuel and M. Endler
Max-Planck-Institut für Plasmaphysik, Euratom Association, 85740 Garching, Germany

C. Ricardi
Dipartamento di Fisica, Universita di Milano, Italy

S. Davies and G. F. Matthews
JET Joint Undertaking, Abingdon Oxon, OX14 3EA, United Kingdom

E. Martines and V. Antoni
Consorzio RFX, Padova, Italy

A. Latten and T. Klinger
Institut für Experimentelle und Angewandte Physik, Kiel, Germany

The rescaled range analysis techniques are used to investigate long-range dependence in plasma edge fluctuations [Mandelbrot and Wallis, Water Resources Res. **4**, 909 (1969)]. This technology has been applied to data from several confinement devices such as tokamaks, stellarators, and reversed-field pinch. The results reveal the self-similar character of the electrostatic fluctuations at the plasma edge with self-similarity parameters ranging from 0.62 to 0.72. These results show that the tail of the autocorrelation function decays as a power law for time lags longer than the decorrelation time and as long as times of the order of the confinement time. In cold plasma devices ($T_e < 1$ eV at the core), there is no evidence of algebraic tails in the autocorrelation function. Some other characteristic features of the autocorrelation function and power spectrum have been investigated. All of these features are consistent with plasma transport as characterized by self-organized criticality. © *1998 American Institute of Physics.* [S1070-664X(98)00510-2]

I. INTRODUCTION

Since the seminal papers of Kolmogorov,[1] the concept of a self-similarity regime in the fluctuations has played a key role in understanding some of the basic features of fluid turbulence. This concept was extended to hydrological data mainly by Mandelbrot[2,3] and later applied to a variety of natural phenomena. Self-similarity of a time series is generally linked to the algebraic decay of the autocorrelation function for long time lags.[4] As a consequence, it can also be linked to long-time dependencies in the dynamics of the fluctuations.

The autocorrelation function of the electrostatic fluctuations at the plasma edge is characterized by a narrow peak around the time lag zero and a slowly decaying tail (that may have oscillations) for large values of the time lag (Fig. 1). The central peak of the autocorrelation function carries information on the correlation of the local fluctuations; the width of the peak measures the decorrelation time of the turbulence. The information on intermediate time scales, between fluctuations and transport phenomena, is brought up by an algebraic falloff from the long-time correlated events. It is in this time scale range that the characteristic time of avalanches and fluctuation modulations should appear. Unfortunately, to accurately determine the tail of the autocorrelation function, high statistics are required. This is a problem for plasma turbulence studies in magnetically confined devices because of the short duration, relative to the confinement time, of the plasma discharges. However, there are techniques that seem to be remarkably effective for the determination of long-range dependencies in a finite time series. One such technique is the rescaled adjusted range statistics (R/S statistics) proposed by Mandelbrot and Wallis,[2] based on the previous hydrological analysis of Hurst.[5] This method leads to the estimation of the Hurst exponent, H, which is related to the fractal dimension of the time series.[6,7]

The existence of long-range time correlations in electrostatic fluctuations at the plasma edge is another argument supporting the idea that self-organized criticality[8] (SOC) is an important mechanism in plasma transport. The concept of
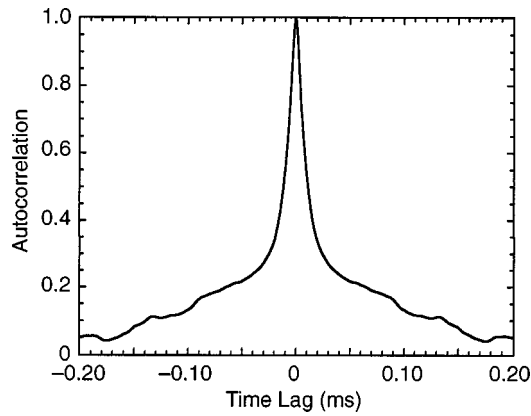
FIG. 1. Autocorrelation function determined from a 50 ms time record of saturation current measurement from shot number 35539 in W7-AS.[32]

SOC brings together ideas of self-organization of nonlinear dynamical systems with the often observed near-critical behavior of many natural phenomena. These phenomena exhibit self-similarities over extended ranges of spatial and temporal scales. In those systems, scale lengths may be described by fractal geometry and time scales that lead to $1/f$-like power spectra. The SOC gives an intimate connection between the scale invariance in space and time.

It has been suggested that the SOC approach could be used to understand some of the observed dynamics in plasma transport.[9,10] Reviews of the initial application of the SOC ideas to plasma confinement and related topics can be found in Refs. 11 and 12. Numerical plasma turbulence calculations[13] that include profile evolution have shown some of the characteristic properties of the SOC systems: the existence of a critical profile gradient and transport by avalanches. There is some indirect experimental evidence for SOC behavior of magnetically confined plasmas in the ''low confinement regime.'' Phenomena such as the resilience of plasma profiles to changes in the location of the heating source, Bohm scaling of the diffusivities, and the apparent nonlocal behavior of some perturbative experiments could be a consequences of SOC dynamics.

We have shown the existence of long-range time correlations in the plasma edge ion saturation current measurements.[14] In this paper, we have done a more complete analysis of the data, extended the analysis to other magnetic configurations and to the floating potential fluctuations. Here, we also describe the statistical techniques used in the determination of the long-range correlations and how to distinguish the long-range turbulence correlations from other plasma physics phenomena, such as coherent modes. We investigate the self-similarity of the edge plasma fluctuations, and we try to identify the self-similarity parameter as a step toward finding the potential role of SOC phenomena in plasma transport. In calculating the self-similarity parameter, we consider Langmuir probe measurements for low-power Ohmically heated or electron-cyclotron-heated (ECH) plasma discharges in several types of confinement devices. We have analyzed data from three stellarators: TJ-IU,[15] Wendelstein 7 Advanced Stellarator (W7-AS),[16] and the Advanced Toroidal Facility (ATF),[17] in the electron cyclotron-

heating (ECH) regime. We have also analyzed fluctuation data records from two tokamaks, TJ-I[18] and the Joint European Torus (JET),[19] in the Ohmic-heated regime, as well as one reversed-field pinch configuration, the Reversed-Field Experiment (RFX).[20] Finally, we have compared these results to the ones obtained from the Thorello device,[21] a toroidal device without rotational transform and with relatively cold plasmas (T_e, $T_i < 1$ eV).

All the comparisons between different magnetic configurations give clear evidence of the existence of long-range correlations in the plasma edge turbulence in confinement devices. This result shows the self-similar nature of the fluctuations. The narrow range of variation of the self-similarity parameter points to a universal character of the dynamics. These results, together with other evidence such as the structure of the fluctuation spectra, support the idea of the SOC character of magnetically confined plasmas.

The rest of the paper is organized as follows. The relation between algebraic tails of the autocorrelation function and the self-similarity of the fluctuations is discussed in Sec. II. The method employed to determine the self-similarity parameter is presented in Sec. III, where the possible source of error in its estimation is also discussed. In Sec. IV, the results of the analysis of experimental data are given and discussed. In Sec. V, some other signatures of SOC found in edge plasma fluctuations are presented. The effect of $\mathbf{E} \times \mathbf{B}$ sheared flow on the self-similarity parameter is shown in Sec. VI. These results are based on a sandpile model, and the possible implications for the experimental data are discussed. Finally, the conclusions of this work are presented in Sec. VII.

II. ALGEBRAIC TAILS IN THE AUTOCORRELATION FUNCTION

In this section, we summarize some of the statistical concepts related to self-similarity and long-range dependence that are the basis for the present studies. Here, we understand by long-range dependence the existence of an algebraic tail in the autocorrelation function. More detailed reviews of these concepts can be found in Refs. 4, 6, 22.

Let us consider a time series of length n, $X \equiv \{X_t : t = 1, 2, ..., n\}$, corresponding to a stationary process. Because this is a finite time series, its mean $\bar{X}(n)$ and variance $S^2(n)$ are well defined. All second-order properties of this time series are given by the autocovariance function $\gamma_\Delta = \text{cov}(X_t, X_{t+\Delta})$, where Δ is the time lag. In terms of the autocovariance, the variance is $V \equiv S^2(n) = \gamma_0$, and the autocorrelation function $\rho_\Delta = \gamma_\Delta / \gamma_0$. An alternative representation of the second-order properties of this series can be constructed through the time series by averaging the original time series over nonoverlapping blocks. That is, for each $m = 1, 2, ..., n$, the new time series is $X^{(m)} \equiv \{X_u^{(m)} : u = 1, 2, ..., n/m\}$, where

$$X_u^{(m)} = \frac{X_{um-m+1} + \cdots + X_{um}}{m}. \tag{1}$$

For each value of m, we can define the autocovariance func-

tion for the $X^{(m)}$ series, $\gamma_\Delta^{(m)} = \text{cov}(X_t^{(m)}, X_{t+\Delta}^{(m)})$, and the corresponding variance $V^{(m)} = \gamma_0^{(m)}$. From these definitions follows Taylor's formula:[23]

$$V^{(m)} = \frac{\gamma_0}{m} + \frac{2}{m^2} \sum_{s=1}^{m} \sum_{\Delta=1}^{s-1} \gamma_\Delta. \tag{2}$$

This relation separates the short and long lag contributions. For a random variable X, the first term dominates. In the limit of large m, we obtain the Gaussian statistics result, that is, the standard deviation decreases as the square root of the number of samples considered. However, for processes with a long-range time dependence, the second term may diverge in the large m limit. In this situation, X does not verify the conditions of the Central Limit Theorem. Equation (2) can also be used to calculate the autocovariance function of the original series in terms of the variance of the successive averaged subseries:

$$\gamma_\Delta = \tfrac{1}{2} \, \delta^2 (\Delta^2 V^{(\Delta)}). \tag{3}$$

Here, the operator δ^2 is the second-order central derivative operator in finite differences,

$$\delta^2(f_i) = f_{i+1} + f_{i-1} - 2f_i. \tag{4}$$

Equation (3) shows that the information on the variance for all of the time series resulting from averaging the original sequence is equivalent to the information contained in the autocovariance function for the original series. Therefore, for an infinite series, $V^{(m)}$ provides an alternative equivalent description of the second-order properties of the original series. However, by formulating the second-order properties in terms of averages over the original time series, we give a higher weight to the low frequencies, and it is possible to do a more accurate estimation of the long-range time dependence.

As previously indicated, in going to the asymptotic limit of $m \to \infty$ for the series considered, there are two possibilities: (1) the second term on the right side of Eq. (2) converges; or (2) the second term on the right side of Eq. (2) diverges. The first case corresponds to the usual Gaussian processes with short-range time dependence. For these processes, as we average over blocks of size m, and the variance decreases as $1/m$. In the second case, the variance decreases slower than $1/m$. Let us consider the case $V^{(m)} = \bar{V} m^{-\beta}$, where $0 < \beta < 1$. In this case, the autocovariance function is

$$\gamma_\Delta \approx \frac{\bar{V}}{2} (2-\beta)(1-\beta)\Delta^{-\beta}, \tag{5}$$

which decays as a power law. It is also straightforward to show that the autocorrelation function for all of the averaged processes is the same, given by

$$\rho_\Delta^{(m)} = \tfrac{1}{2} \, \delta^2 (\Delta^{2-\beta}). \tag{6}$$

Because all of the averaged processes have the same autocorrelation function, the original series is called self-similar. This definition is equivalent to the more intuitive one; that is, the process X is called second-order self-similar with self-similarity parameter $H = 1 - \beta/2$, if, for all $m = 1,2,3,...,n$ $(X_{tm-m+1} + \cdots + X_{tm})/m^H$, $t = 0,1,2,...$, has the same vari-

ance and autocorrelation as X. The parameter H is the self-similarity parameter, and it is also called the Hurst parameter. In general, Eq. (6) is only verified for large time lags, and self-similarity is taken as an asymptotic property of the time series.

To accurately determine the tail of the autocorrelation function and the parameter H, very high statistics are required. This creates a problem for plasma turbulence studies in magnetically confined devices because of the short duration of the plasma discharges. However, there are techniques that seem to be effective for the determination of H in a finite time series. One such technique is the R/S statistics proposed by Mandelbrot and Wallis[2] and is based on the previous hydrological analysis of Hurst.[5]

The R/S ratio is the ratio of the maximal range of the integrated signal normalized to the standard deviation. It is defined as

$$\frac{R(n)}{S(n)} = \frac{\max(0,W_1,W_2,...,W_n) - \min(0,W_1,W_2,...,W_n)}{\sqrt{S^2(n)}}, \tag{7}$$

where

$$W_k = X_1 + X_2 + \cdots + X_k - k\bar{X}(n). \tag{8}$$

For a sequence with short-range dependencies, of which a random signal is an extreme case, the expected value of this ratio scales as

$$E\left[\frac{R(n)}{S(n)}\right] \xrightarrow[n \to \infty]{} \lambda n^{0.5}. \tag{9}$$

Here, $E[x]$ is the expected value of the variable x. For phenomena characterized by a long-range time dependence, the expected value of R/S scales as

$$E\left[\frac{R(n)}{S(n)}\right] \xrightarrow[n \to \infty]{} \lambda n^H, \tag{10}$$

with $H \neq 0.5$. For $1 > H > 0.5$, there are long-range time correlations for $0.5 > H > 0$, the series has long-range anticorrelations, and if $H = 1.0$, the process is deterministic. The H used here is the same Hurst parameter introduced previously. A constant H parameter over a long range of time lag values is consistent[4] with the self-similarity of the signal and an autocorrelation function given by Eq. (6). In comparison to the direct determination of the autocorrelation function or other alternative techniques of calculating the value of H, the R/S analysis is remarkably robust.[24]

III. DETERMINATION OF THE SELF-SIMILARITY PARAMETER

There have been many detailed studies of the reliability of the R/S method to calculate long-range correlations. In general, it is difficult to do so because it is difficult to separate the robustness of the analysis method from the accuracy of the method to generate a self-similar time series with a given self-similarity parameter. In many instances, the problems found with this method are related to the length of the samples used. In particular, in medical and economic studies

Phys. Plasmas, Vol. 5, No. 10, October 1998

Carreras *et al.*   3635

TABLE I. An *R*/*S* analysis of sequences of random data.

Points in the time series	Averaged *H*	Standard deviation
10^3	0.543	0.054
10^4	0.556	0.012
10^5	0.529	0.008
10^6	0.524	0.003

with intrinsically limited series lengths, this is a major source of concern.[25–27] In those instances, we are referring to a series of less than 1000 points. Fortunately, this is not the case in the fluctuation samples that we have considered. Our concern in using this method is not only with its accuracy but also with plasma phenomena that could distort or mask the proper determination of *H*. In this section, to verify the robust character of the *R*/*S* analysis for the plasma fluctuation data and eliminate the contamination by other effects, we consider some typical examples of fluctuation data and data produced by simple dynamical models. We also investigate the contamination of the measurement by noise.

To calculate *R*/*S*, we use the method outlined in the previous section. For a given data set, we subdivide the data in nonoverlapping blocks, calculate *R*/*S* for each block, take proper averages, and plot the results as a function of the lag in a log–log plot. Error bars are estimated from the dispersion of the *R*/*S* values given by each block. The last few points on the high-lag end of the plot are not taken into consideration because they lack statistical significance. This is because the size of the blocks is of the order of the size of the time sample. In plasma physics applications, the lower end is linked to the correlation time of the fluctuations, and we also do not take this into consideration.

First, we would like to illustrate the issue of the accuracy of the method. To do so, we consider the case of random noise. In this case, the signal is uncorrelated, and the decay indices should be $\beta = 1$ and $H = 0.5$. Using the random number generator from the NAG library, we have generated 100 time series of 10^6 points each. We have analyzed sequences of $10^3 - 10^6$ in length. The results of the *R*/*S* analysis are shown in Table I. In the table, the averaged value of *H* over the different realization is shown together with the standard deviation. The averaged value of *H* converges to a 0.52 value for time series with more than a ten thousand points. The value of *H* is not the expected 0.5 value. The discrepancy may be caused by both an accuracy problem of the *R*/*S* analysis and/or the random number generator. These calculations can give us guidance in the determination of the existence of a long-range correlation when compared with the analysis of fluctuation data.

It is interesting to consider the case of a time series, created by an oscillatory motion, that is, a pure sine function. This series results from deterministic dynamics. If the time discretization is much smaller than the period, the time trace is a continuous curve. Therefore, the expected Hurst exponent is 1. In Fig. 2, we have plotted the *R*/*S* values for a sinusoidal signal of 100 000 data points with a period of 1000 points. For lags up to the value of the period, the Hurst exponent is $H = 1.0$, as expected; for longer lag values, *H*
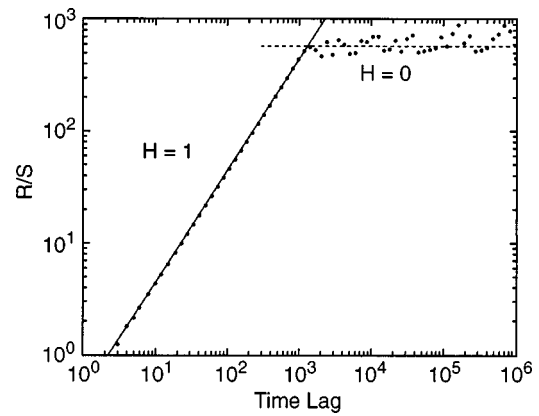

FIG. 2. We see *R*/*S* as a function of time lag for a sinusoidal signal of 100 000 data points with a period of 1000 points.

≈ 0.0 in an averaged sense. This result can be extended to *any* periodic signal. Therefore, the presence of coherent oscillation, a coherent mode, and/or a pure wave appears as a clear pattern in the *R*/*S* plot.

For a coherent mode, we expect a signature in the *R*/*S* plot similar to the periodic signal just considered. The effect of coherent modes is clearly seen in some experimental Langmuir probe data from the KIWI Linear device,[28] where drift waves are destabilized.[29,30] When an $m = 2$ drift mode is established, the probe data has a spectrum with very strong peaks at 13 kHz and its harmonics at 26, 39, and 52 kHz. It also has weak peaks at 6.5, 19.5, 32.5, and 45.5 kHz (subharmonics due to the presence of a weak mode-locked $m = 1$ mode). The *R*/*S* plot for these data is shown in Fig. 3. In going from small to large lags, we have an initial ramp with $H = 1.0$. Then there is an abrupt flattening to $H = 0.0$ at lag of about 20, definitely corresponding to the main harmonic of 13 kHz; an exact correspondence would give a turnover at lag 19. Then there is an intermediate zone with $H = 0.77$, followed by a gradual rise to $H = 1.0$ at a time lag of about 700. Finally, a turnover to $H \approx 0.5$ occurs at a lag of around 5000. This last turnover is identified as a 50 Hz (=5000 points) component, which is also noticed in the fluctuation power spectrum. The *R*/*S* analysis clearly points to the exis-
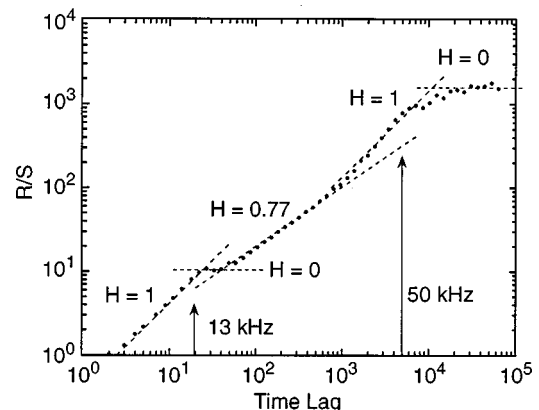

FIG. 3. We see *R*/*S* as a function of time lag for probe measurements from the KIWI Linear device.[28] The figure shows the presence of at least two coherent modes for this discharge.
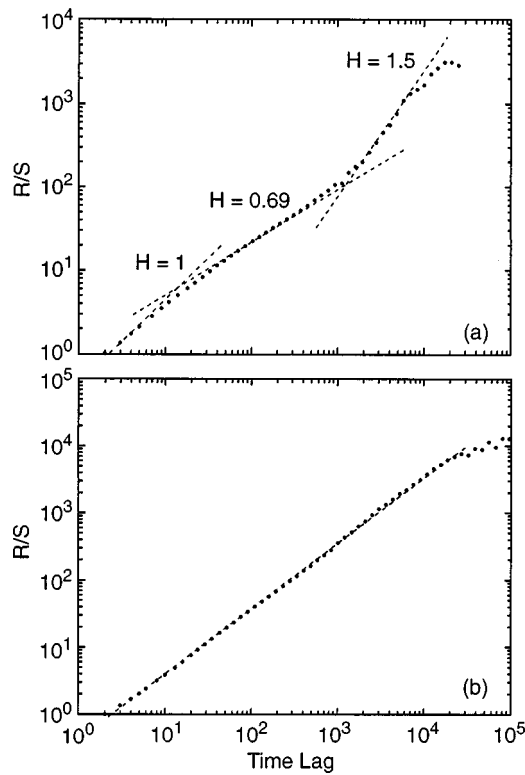
FIG. 4. We see R/S as a function of time lag for (a) a reciprocating probe measurement (shot 39650-23) and (b) a fixed probe measurement (shot 3474-11) in the JET device and outside the last close flux surface.[35]

tence of coherent modes. Under these circumstances, it is not possible to make a quantitative evaluation of the long-range correlations in the background turbulence.

A sharp rise of R/S as a function of lag can also be caused by a coherent flow such as a plasma drift or by the motion of the probe. When reciprocating Langmuir probes are used, the motion of the probe can be detected at large time lags. In Fig. 4(a), we show an R/S plot for fluctuations measurement with a reciprocating Langmuir probe in JET. The velocity of the probe is 1 m/s. After an initial slope of $H = 1.0$, it settles down to $H = 0.7$. At a lag of about 1500, the slope rises to a value well above 1.0. Such a fast rise is not seen by a fixed divertor probe for the shot with similar parameters [Fig. 4(b)].

Values of H greater than 1 can only be attained transiently for values of the time lag less than L_n/V_p and when the effect of the drift is close to the amplitude of the fluctuations. Here, L_n is the profile scale length, and V_p is the velocity of the probe. We have created sequences of data combining random noise with a drift represented by a sinusoidal function of time. The R/S plot obtained in each case is similar to Fig. 4(a). If we calculated the H value in the fast raising phase, we see that it is a strong function of the ratio of the amplitude of the sinusoidal signal to the random one (Fig. 5). For a narrow window of values for this ratio, H is greater than unity. In the two asymptotic limits, noise dominating and sinusoidal dominating, one obtains the values discussed previously.

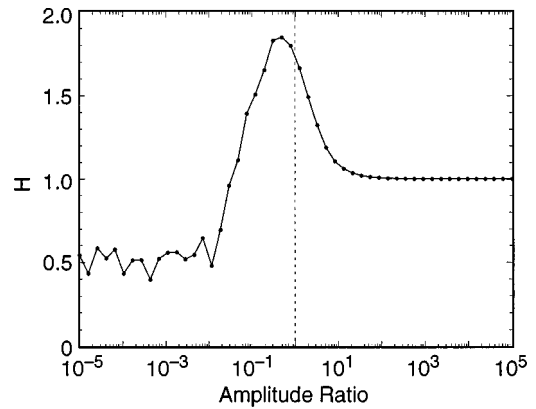Let us now consider a more complicated deterministic dynamical model that can give further insight on the infor-

FIG. 5. The Hurst exponent calculated on the fast rising phase of R/S for a sequence of a time series combining a sinusoidal signal of period 10^5 with random noise. Here H is plotted versus the ratio of the amplitude of the former to the latter. The sequences have 10^5 points and the fast rising phase is for time lags between 4000 and 300 000.

mation carried out by the R/S analysis. The Lorenz model is a simple dynamical model with complex behavior.[31] This system is defined by the equations

$$\frac{dx(t)}{dt} = \sigma[y(t) - x(t)], \tag{11}$$

$$\frac{dy(t)}{dt} = -x(t)z(t) + rx(t) - y(t), \tag{12}$$

$$\frac{dz(t)}{dt} = x(t)y(t) - bz(t). \tag{13}$$

We have analyzed solutions of this model using the R/S statistics. In Fig. 6, we have plotted a case with the parameters $\sigma = 16.0$, $r = 45.92$, and $b = 4.0$. The Lorenz equations have been solved from the initial point (17.83, 12.34, 10.32) by integrating with time steps $\Delta t = 0.02$ using a Runge–Kutta integration method. This generates an attractor with dimension $d = 2.06$. We have analyzed the series $y(t)$. The results shown in Fig. 6 give an initial slope at $H = 1.0$ that turns gradually over to $H = 0.5$ for long time lags, indicating that the "memory" of this signal is about 200 points. We can see the same type of effect by considering two-
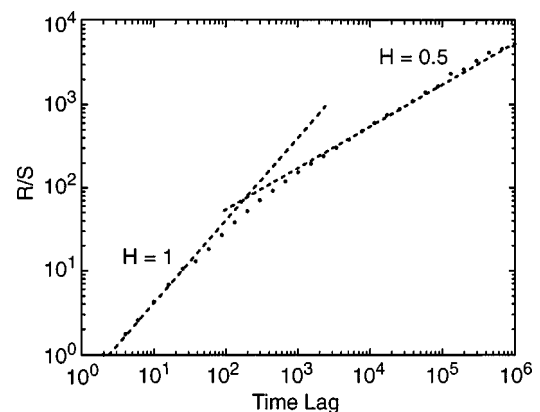

FIG. 6. We see R/S as a function of the time lag for the $y(t)$ series of the Lorenz model, Eqs. (11)–(13).
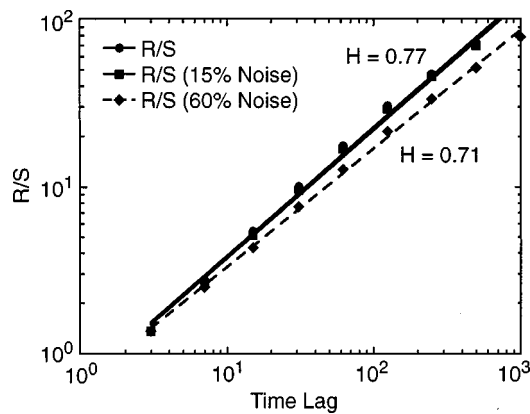
FIG. 7. The effect on R/S of adding random noise to a edge probe measurement from the TJ-I device (Ref. 18). A sample of 10 000 points have been used in this calculation.

FIG. 8. A test of the R/S determination by creating a new series randomizing the time sequence of the data. The calculated Hurst exponent for the surrogate series is compared to the exponent of the original series. The time series are from the RFX plasma edge measurements.

dimensional plots of $y(t)$ vs $y(t+\Delta)$, where Δ is a time lag. For values of Δ below 200, we obtain a projection of the Lorenz attractor. However, for larger lags the trajectory is area filling.

All the potential problems in the determination of H discussed in this section, such as the existence of coherence oscillations and/or plasma drifts, produce a clear signal in the value of R/S. Although they are distinct from long-range dependencies in the turbulence, they do not allow the extraction of the value of H. A careful selection of the data is needed to avoid samples dominated by plasma drifts and magnetohydrodynamic (MHD) phenomena. However, these phenomena do not produce misleading interpretations for H because they carry clear signatures that allow the exclusion of data that do not provide information on the plasma turbulence. The consistent determination of H has also been cross-checked with the determination of the scaling with the time lag of the variance and probability of return.

We have further tested the robustness of the R/S estimate by adding random noise to a signal. To do so, we have selected one of the TJ-I sets of data, 10 000 points, and have added different levels of random noise. In Fig. 7, the plot for three cases is shown. The levels of added noises are 0%, 15%, and 60%. Even with 60% noise, the Hurst parameter hardly changes. With a 15% added noise level, the difference is undetectable, and for 60% noise, the Hurst parameter changes by 6.6%. This gives a good measure of the robustness of this technique.

Finally, to find a good criterion to distinguish between weak correlations and no correlation, we have used a common technique applied to the analysis of dynamical systems. For each time series, we can create a surrogate time series. This new series is created by randomizing the time sequence of the data. This eliminates the time correlations. We calculate the Hurst exponent for the surrogate series and compare it to the exponent of the original series. In Fig. 8, we show an example based on the time series from RFX plasma edge measurements. There is a clear distinction between the exponents of the original series and the surrogates; this difference indicates that there are long-range correlations in the original data.
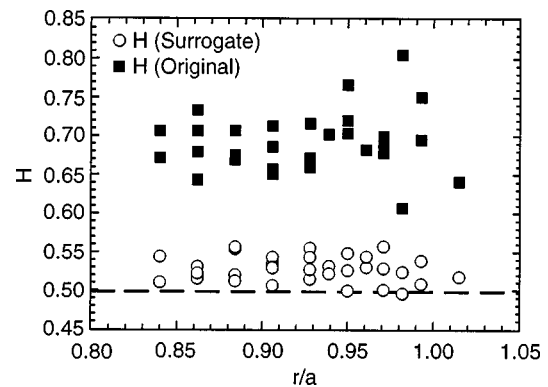
The robust character of the calculation of H is also evident by the reproducibility of the results. The radial profiles of H for discharges with the same parameters are very similar. Although the error bars for individual points in many cases may be comparable to the radial variation of H, the radial profiles are reproducible.[14]

IV. R/S ANALYSIS OF THE EXPERIMENTAL RESULTS

In the present study, the data analyzed are edge Langmuir probe measurements from three stellarators, TJ-IU,[32] W7-AS,[33] and ATF,[34] in the ECH heated regime; two tokamaks, TJ-I[18] and JET,[35] in the Ohmic heated regime; and one reversed-field pinch, RFX.[36] We have compared these results to the ones obtained from the Thorello device,[21] a toroidal device without rotational transform and relatively cold plasmas. The available data correspond to radial probe scans with positions that are close to, and within, the edge sheared flow layer. A summary of the main parameters of these devices and of the discharges analyzed here are given in Table II. In the table, R is the major radius of the device, $\bar{a}$ is the averaged plasma minor radius, $\bar{n}_e$ is the averaged plasma density, B_T is the toroidal magnetic field, and P is the ECH power.

For ion saturation current fluctuation measurements at the plasma edge, a typical plot of R/S versus time lag is shown in Fig. 9. For time lags smaller than a few decorrelation times, there is a transient with a nearly constant slope, generally with a value close to 0.9. After this initial phase, R/S settles on an ''asymptotic'' power law that is used to determine the value of H. The range of the time lags over which H is determined is the ''self-similarity range'' given in Table III for each dataset. Typically, the value of the self-similarity range is several orders of magnitude longer than the turbulence decorrelation time, and in most cases the upper limit given in Table III is set by the availability of data. In Table III, we also give the turbulence decorrelation time, τ_D. The turbulence autocorrelation time is estimated at the zero velocity point in the shear layer for each dataset.

The main result of our analysis is that, for all datasets, the Hurst parameter is constant and well above 0.5 over a

TABLE II. Data analyzed.

Device	Number of time series	R (m)	$\bar{a}$ (m)	$\bar{n}_e$ (m^{-3})	B_T (T)	ECH P (kW)
TJ-I	9	0.30	009.5	$(1-2)\times10^{19}$	0.8–1.0	
JET	8	2.85	$a_0=0.95$ $b/a_0=1.85$	$(1-2)\times10^{19}$	2.6	
TJ-IU	21	0.60	0.1	$(1-5)\times10^{18}$	0.67	200
W7-AS	53	2.00	0.2	$(1-2)\times10^{19}$	1.25–2.5	
ATF	20	2.10	0.27	$(3-6)\times10^{18}$	1.0	200–400
RFX	29	2.00	0.457	$(3-5)\times10^{19}$	$B_p=0.15-0.2$ T	
Thorello	10	0.40	0.08	10^{16}	0.2–0.1	

self-similarity range much longer than the turbulent autocorrelation time. This result is a clear indication of the existence of long-range dependencies in the fluctuation dynamics. Because the self-similarity range involves time lags from the fluctuation time scales to transport time scales, it is also an indication that there is no clear separation of time scales between the fluctuation and the transport dynamics. In Table III, $\langle H \rangle_{in}$ is the radial average of H in the plasma edge within the last flux surface; and $\langle H \rangle_{out}$ is the radial averaged of H in the scrape-off layer (SOL). The $\pm$ indicates the radial variation of H; it is not an error bar. Within the plasma, the averaged Hurst parameter varies between 0.62 and 0.72, a relatively small range given the diversity of plasma confinement devices considered. Partial results of this analysis were presented in Ref. 14. In some cases, the numerical values of H may be slightly different because here we have chosen the self-similarity range in a more consistent manner. In Fig. 10, we have plotted the radial profile of H for the different magnetic configurations. We use as the ''radial'' variable, x, the distance in real space between the position of the probe and the zero-velocity point in the shear flow layer, and we do not take into account the geometry of the flux surfaces. Positive values of x correspond to the edge plasma region. We have only plotted the H profile from the last closed flux surface up to 3.5 cm within the plasma. We can see that the distribution of values is relatively similar for the three types of magnetic configurations considered.
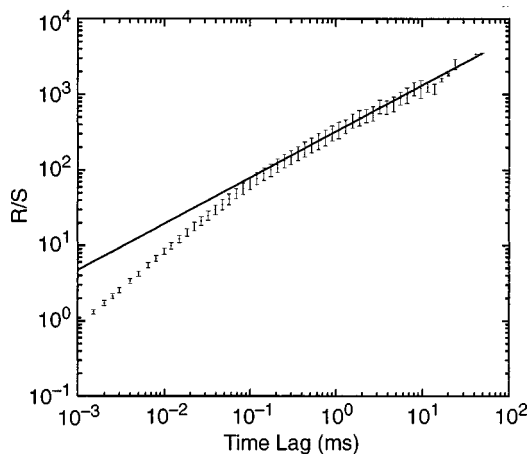

FIG. 9. A plot of the expected value of R/S as a function of the time lag for the same time record of W7-AS as in Fig. 1 (Ref. 33).

The situation is, however, quite different in the scrape-off layer (SOL). In the SOL, the values of H have a broader range of variation. This variation could reflect the diversity of SOL conditions for the devices considered. For instance, we can see from the JET results in Table III that the value of H in the SOL changes considerably from a limiter configuration to a divertor configuration. These data are from the same shot. For this discharge, JET was operated initially in a limiter configuration and later switched to a divertor configuration. In Ref. 14, we also showed the large scatter of H values for the different SOL structures in the stellarators. The fact that H in the SOL varies from device to device is an indication of the lack of universality in the plasma behavior in the SOL. This result is not surprising. We should not expect much SOC behavior to hold within the SOL. Moving into the SOL, the outward flux changes from perpendicular to parallel and the radial flux bursts[36] will change to parallel flux burst. An issue is how far from the last flux surface the system begins to lose the SOC character.

The results of tokamaks, stellarators, and RFP contrast with the ones obtained in the analysis of fluctuations in the Thorello device. Thorello[21] is a toroidal device without rotational transform; its main parameters are given in Table II. It is capable of producing hydrogen magnetized plasma in a steady-state condition. The plasma is obtained by using one or more tungsten wires, placed in the inner part of the torus and negatively biased ($V = -100$ V) with respect to the chamber walls. In this device, there is neither a transformer to induce a toroidal current nor external auxiliary coils to produce a poloidal magnetic field. Typical plasma parameters are the following: $T_e = 1$ eV and $T_i = 0.3$ eV, plasma density at the edge is 10^{15} m^{-3}, and at the center 10^{17} m^{-3}. The data for the present analysis were obtained by Langmuir probes in the center plasma column and by varying the neutral gas pressure (from 10^{-4} to 6×10^{-4} mbar) and the toroidal magnetic field (from 1 to 2 kG). The values of the H parameter for ten different time series are plotted in Fig. 11. They are compared to the values of H for the corresponding surrogate series. We can see that within the error bars the Hurst parameter shows very little or no long-range correlations for these measurements.

The analysis up to now has been limited to the saturation current fluctuations at the edge. A similar treatment has been applied to the floating potential. In spite of the differences in the wave forms between the ion saturation current fluctua-

TABLE III. A summary of the analysis results.

Device	Number of time series	$\langle H \rangle_{in}$	$\langle H \rangle_{out}$	τ_D (μs)	Self-similarity range (ms)
TJ-I	9	0.64 ± 0.03	0.70 ± 0.04	3.0	0.02–1.0
JET limiter	4	$\cdots$	0.52 ± 0.04	29.0	0.1–2.0
JET divertor	4	$\cdots$	0.63 ± 0.03	19.0	0.1–2.0
TJ-IU	21	0.64 ± 0.03	0.67 ± 0.01	6.0	0.1–2.0
W7-AS $\iota_a=0.243$	24	0.62 ± 0.01	0.60 ± 0.04	20.0	1–20
W7-AS $\iota_a=0.355$	29	0.72 ± 0.07	0.66 ± 0.06	19.0	1–20
ATF	20	0.71 ± 0.03	0.92 ± 0.07	34.0	1–12
RFX	29	0.69 ± 0.04	$\cdots$	3	0.03–3.0
Thorello	10	0.55 ± 0.04	$\cdots$	6	0.05–5.0

tions and floating potential fluctuations, as we have discussed elsewhere,[37] the values of H are very close (Fig. 12). Within the expected error bars of the calculation, we cannot identify any different trends or levels between both types of measurements. The results plotted in Fig. 12 are from the TJ-IU torsatron. Negative values of x correspond to the SOL and positive values to the plasma edge region.

V. EVIDENCE FOR SOC BEHAVIOR OF PLASMA TRANSPORT IN THE EDGE FLUCTUATION MEASUREMENTS

The results of the analysis of edge fluctuation data presented in the previous section clearly shows the existence of long-range correlations in most of the time records examined. However, it is important to realize that the fluctuation measurements used in the present analysis correspond to plasmas with a differential rotation in the poloidal direction with respect to the laboratory frame. The long-range dependencies identified here may not necessarily be long range in time; they could be the reflection of long-range dependencies in the poloidal variable. Because these edge flows have

shear, it is not possible to resolve this ambiguity by analyzing data taken at the position of zero flow. As we discuss in the next section, numerical calculations indicate that shear flows may suppress the long-range correlations. The position of zero flow is normally close to the position of maximum shear. Therefore, it is not clear what causes the changes observed in this position. From the perspective of detecting signatures of SOC behavior in plasma transport, the distinction between long-range time and poloidal correlations is less important. In either case, the presence of such dependencies is consistent with plasma transport mechanisms based on avalanches.

The absence of long-range correlations in the Thorello device can be a further indication that these correlations are caused by the existence of a critical point that may be related to the level of power in the device, and it is not an intrinsic characteristic of all plasma fluctuations.

Another interesting signature of a SOC system is the fluctuation and flux spectrum. It is necessary to calculate the spectra in the plasma reference frame; otherwise, the spectral decay indices may be meaningless, or at least difficult to
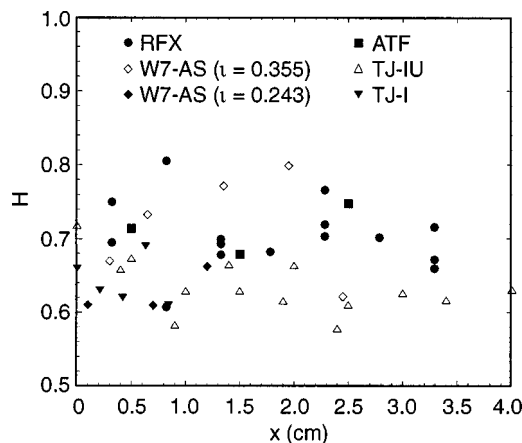

FIG. 10. The radial profile of the Hurst parameter H within the last flux surface for several of the devices considered in this paper.
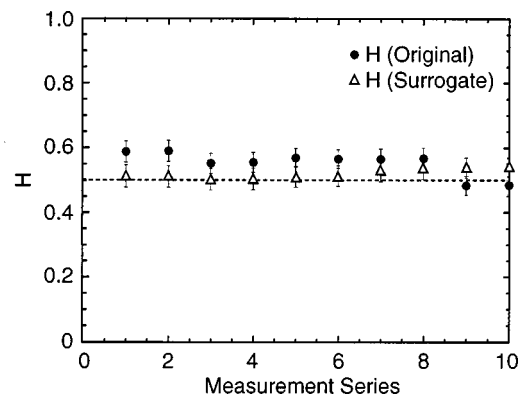

FIG. 11. Hurst parameter H for several plasma discharges in the Thorello device (Ref. 21) compared with the values obtained for the corresponding surrogate sequences. These results show the short-range correlation of the fluctuations in this device.
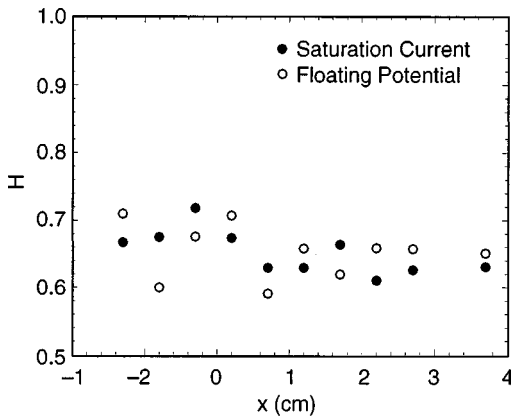
FIG. 12. The radial profile of *H* for the ion saturation current and floating potential fluctuations. The time series are from a sequence of discharges in the TJ-IU torsatron.

FIG. 14. The autocorrelation function for edge fluctuation data from W7-AS calculated every 1 ms (Ref. 33). The plot shows the time evolution over a 50 ms interval. It shows intermittent increases of the tail of the autocorrelation function and is correlated with increases of the *H* parameter.

interpret. Here, we have calculated the spectra around the position of zero flow. In Fig. 13, we have plotted the spectrum of the ion saturation current fluctuations from W7-AS data. The spectrum is calculated using a record of length 20 ms, and it is averaged using data from three reproducible discharges. This spectrum strongly resembles the ones obtained in simple sandpile calculations,[10,38] as well as those obtained in turbulence model realizations of SOC systems.[13,39] The spectrum shows three regions with approximate decay indices that are consistent with 0, −1, and −4, respectively. Very similar results were first obtained in DIII-D discharges.[40]

Calculating the autocorrelation function for the W7-AS data in records of 1 ms, we can study its evolution over a 50 ms interval (Fig. 14). The 2-D plot shows intermittent increases of the tail of the autocorrelation function. Different possible mechanisms can explain this phenomena. One is the effect of transport avalanches as a similar signature, as is seen in SOC models. However, because of the plasma rotation, it also could be caused by correlated blobs moving in the poloidal direction. Because the information that we can

extract with a single probe is very limited, the use of multiple probes could be a way of discerning between these possible explanations.

The results of this analysis show that the plasma edge turbulence is consistent with the SOC paradigm of turbulent transport. However, it does not prove that this model offers the only explanation for the experimental observations. At this point, we are not aware of other dynamical mechanisms that may provide an alternative answer, but it may exist. More detailed experimental tests, mainly involving radial correlation measurements, are needed.

VI. EFFECT OF SHEARED FLOWS ON THE SELF-SIMILARITY PARAMETER

In this section, we explore the possible consequences of the presence of a sheared flow on the long-range correlations. To do so, we first need a dynamical model. Cellular automata with rules based on the sandpile dynamics have been a standard model in studying generic properties of SOC.[8,38] The model is based on the existence of a critical sandpile slope. When, by random addition of grains of sand, the critical slope is reached, grains of sand fall down the pile in a prescribed manner. The dynamical process shows that in a steady state the sandpile slope is in the averaged sense well below the critical slope and yet the transport of sand is still produced by avalanches. These avalanches have length scales from a single cell to the full size of the system. Here, we consider a 2-D sandpile model with the added effect of sheared wind. The particular algorithm used for the sandpile evolution in the present calculations was explained in detail in Ref. 41. Here we present only some of the results of this model.
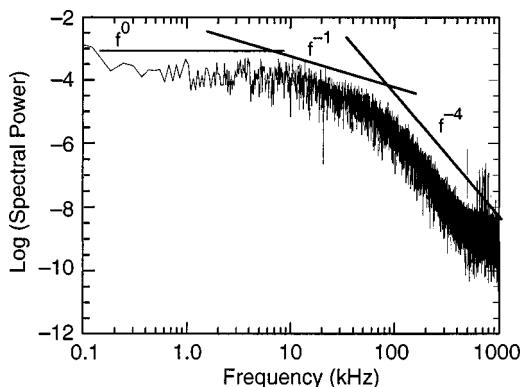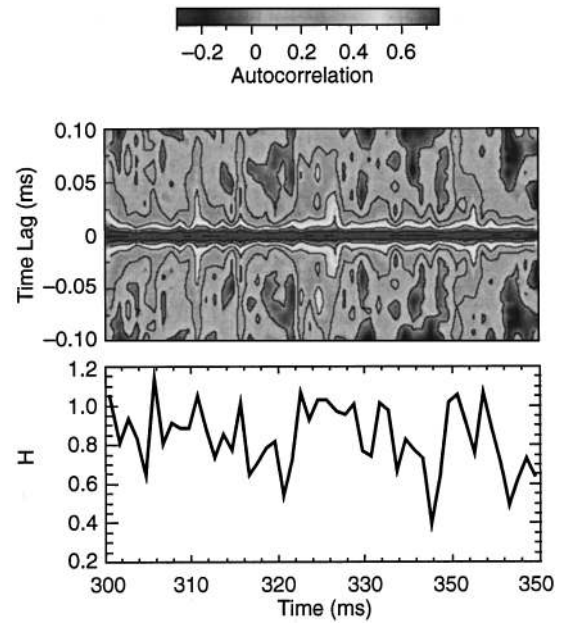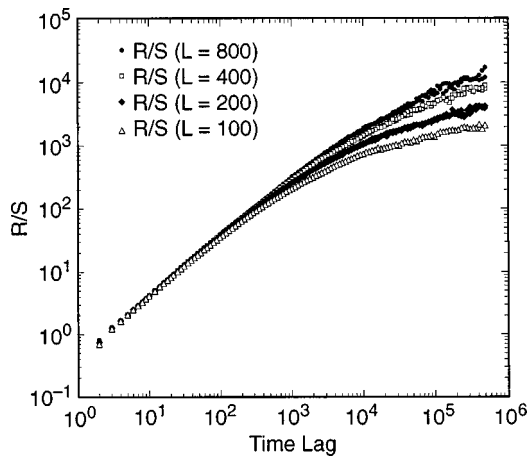

FIG. 13. The ion saturation current spectrum for a W7-AS discharge at the radial position where the flow velocity is zero (Ref. 33). We use a record of length 20 ms, and the spectrum is averaged over three reproducible discharges. The structure of the spectrum is similar to the characteristic spectrum from sandpile models.

Phys. Plasmas, Vol. 5, No. 10, October 1998

Carreras *et al.*   3641

FIG. 15. We see *R/S* versus the time lag for four different values of the sandpile length, *L*. They show that the turning over of *R/S* is a function of *L*.

FIG. 17. The addition of a sheared flow to the sandpile induces a decorrelation of avalanches (Ref. 41). This decorrelation effect is shown by the change in the value of *H*.

We have applied the *R/S* analysis to time sequences of sandpile data. The particular data sequences are the total number of cells overturning in each time step. This quantity, normalized to the total length of the sandpile, can be taken as the radial averaged particle flux. The calculations have been carried out in a regime of weak avalanche overlap and they give a constant value of *H* over many decades. This value is around 0.8, with slight variation from case to case depending on the probability of adding grains to the sandpile. The number of decades over which the Hurst exponent is constant scales with the length of the sandpile. This effect is illustrated in Fig. 15, where *R/S* versus the time lag has been plotted for four different values of the sandpile length, *L*. To clearly see the effect of the size of the sandpile on the scaling of *R/S*, we have subtracted to the *R/S* values plotted in Fig. 15 a power fit made to the lower range of time lags. The deviation from this fit is plotted in Fig. 16. We can see that the time lag when the deviation begins increases significantly with *L*.

As shown by previous calculations, the addition of a sheared flow to the sandpile induces a decorrelation of avalanches.[41] This decorrelation effect is clearly demonstrated by the change in the value of *H*. When a sheared flow is added to the sandpile, the long-range correlations are eliminated, and *H* is close to 0.5 (Fig. 17).

The effect of reducing *H* by shear flow for large values of the time lag is different from the effect, first determined in the Texas Experimental Tokamak (TEXT)[42] and later seen in other devices,[43] of the reduction of the decorrelation time of the turbulence. The reduction of *H* at large time lags is the result of the decorrelation of avalanches. The value of shear flow that causes such decorrelation is possibly too low to cause any effect on the fluctuations. The avalanche decorrelation should result in a change on the confinement scaling (from Bohm to gyro-Bohm). This effect is not necessarily directly measured as an increase in the confinement time. However, the reduction of the decorrelation time of the turbulence causes a direct increase in confinement time. This is an effect predicted by theory.[44] Experimental observations show correlation between the effect of **E**×**B** shear flows and the reduction of turbulence.[43,45] There are not yet experimental analysis of the effect of the shear flow on the long-time correlation of turbulence.

There is some indication in the analyzed data that the reduction of long-range correlations by **E**×**B** sheared flow effect could also be present at the plasma edge turbulence. In W7-AS, a small reduction of *H* is near the shear layer. This effect is weak, and it is not possible to distinguish it from other effects such as the transition from poloidal correlation to time correlations caused by the change in velocity. Other effects may also be present in crossing to the SOL. Not all the profile changes are aligned with the zero of the shear flow, however, we have not measured directly the plasma flow. The shear flow layer is defined from the measurement of the phase velocity of the fluctuations and the maximum shear in the **E**×**B** flow may be somewhat displaced. Again, a single probe measurement is a limitation that does not always allow separation between the different effects present at the plasma edge.
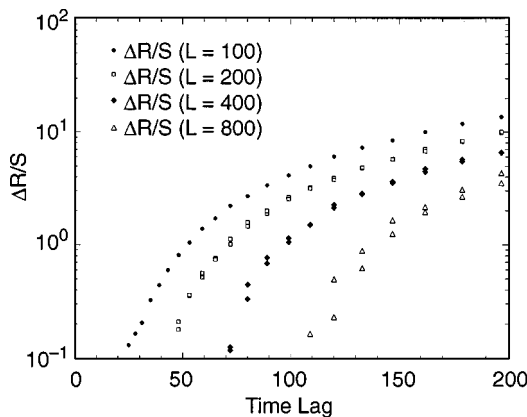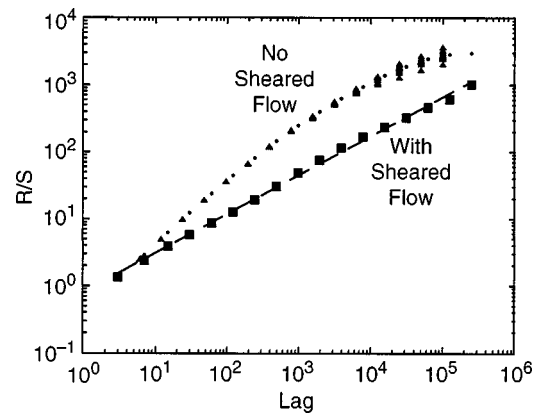

FIG. 16. For the same data of Fig. 15, this plot shows the value of the time lag at which the slope of *R/S* changes. It increases linearly with the length of the sandpile.

VII. CONCLUSIONS

The analysis of the edge plasma fluctuations in several confinement devices indicates that the fluctuations have self-similarity character over a broad range of time lags. Therefore, long-range time correlations are present, and the tail of the turbulence autocorrelation function decays as a power law for time lags longer than the decorrelation time and up to times of the order of the confinement time. However, because of the presence of sheared flows, it is not possible to separate between time and poloidal long-range correlations.

The self-similarity parameter within the last flux surface falls into a narrow range of values, from 0.6 to 0.72. Over this range, the values for the different devices considered strongly overlap. That is the radial variation of an *H* for a type of magnetic configuration is comparable to the variation found among different magnetic configurations. These results point to a universal character of the mechanism responsible for the long-range correlations.

Fluctuation spectra measured at the position of zero velocity have decay indices that are consistent with the one obtained in SOC models. A systematic study of the spectra is underway, and it will be discussed in a future publication.

Calculations show that long-range time correlations are reduced or even eliminated by a shear flow effect. In the experiment, the sheared flows are not strong enough to suppress turbulence, but there are indications that the long-range time correlations are modified by a shear flow. Unfortunately, however, the problem of separating between sheared flow effects and changes because of the motion of the reference frame cannot be resolved with these single probe measurements.

These results are consistent with SOC behavior and plasma transport mechanisms based on avalanches. A more systematic analysis of data from other confinement devices is needed to confirm these conclusions. In particular, measurements comparing long-range radial correlations should be compared with long-range time correlations.

ACKNOWLEDGMENT

[1] U. Frisch, *Turbulence, the Legacy of A. N. Kolmogorov* (Cambridge University Press, Cambridge, 1995).

[2] B. B. Mandelbrot and J. R. Wallis, Water Resour. Res. **4**, 909 (1969).

[3] B. B. Mandelbrot and J. R. Wallis, Water Resour. Res. **5**, 422 (1969).

[4] G. Samorodnitsky and M. S. Taqqu, *Stable Non-Gaussian Random Processes: Stochastic Models with Infinite Variance* (Chapman and Hall, New York, 1994).

[5] H. E. Hurst, Trans. Am. Soc. Civ. Eng. **116**, 770 (1951).

[6] J. B. Bassingthwaighte, L. S. Liebovitch, and B. J. West, *Fractal Physiology* (Oxford University Press, New York, 1994).

[7] J. G. Moreira, J. K. L. da Silva, and S. O. Kamphorst, J. Phys. A **27**, 8079 (1994).

[8] P. Bak, C. Tang, and K. Weisenfeld, Phys. Rev. Lett. **59**, 381 (1987).

[9] P. H. Diamond and T. S. Hahm, Phys. Plasmas **2**, 3640 (1995).

[10] D. E. Newman, B. A. Carreras, P. H. Diamond, and T. S. Hahm, Phys. Plasmas **3**, 1858 (1996).

[11] B. A. Carreras, D. Newman, V. E. Lynch, and P. H. Diamond, Plasma Phys. Rep. **22**, 740 (1996).

[12] R. O. Dendy and P. Helander, Plasma Phys. Controlled Fusion **39**, 1947 (1997).

[13] B. A. Carreras, D. E. Newman, V. E. Lynch, and P. H. Diamond, Phys. Plasmas **3**, 2903 (1996).

[14] B. A. Carreras, B. Ph. van Milligen, M. A. Pedrosa, R. Balbín, C. Hidalgo, D. E. Newman, E. Sánchez, M. Frances, I. García-Cortés, J. Bleuel, M. Endler, S. Davies, and G. F. Matthews, Phys. Rev. Lett. **80**, 4438 (1998).

[15] E. Ascasibar, C. Alejaldre, J. Alonso, F. de Aragon, R. Balbin, B. Brañas, E. de la Cal, F. Castejon, J. Castrejon, G. Catalan, J. R. Cepero, T. Estrada, R. Fernandez, M. Frances, J. de la Gama, L. G. Gonzalo, I. G. Cortes, G. Gomez, J. Guasp, J. Herranz, C. Hidalgo, J. A. J. Aparicio, A. Jimenez, V. Krivenski, I. Labrador, F. Lapayese, M. Liniers, A. L. Fraguas, J. L. Razola, A. L. Sanchez, E. de la Luna, R. M. Garcia, E. M. Roquero, L. M. Martinez, F. Medina, M. Medrano, B. Ph. van Milligen, M. A. Ochando, P. Ortiz, L. Pacios, L. Pallas, I. Pastor, M. A. Pedrosa, J. Qin, M. C. R. Fernandez, L. R. Rodrigo, F. Rufino, A. Salas, L. S. Cabezudo, A. S. Corpas, E. S. Gonzalez, J. S. Sanz, C. Sierra, F. Tabares, D. Tafalla, V. Tribaldos, A. Varias, J. Vega, B. Zurro, L. M. Kovrizhnykh, D. C. Akulina, O. F. Fedyanin, L. V. Kolik, K. M. Likin, Y. I. Nechaev, A. E. Petrov, K. A. Sarksyan, N. V. Matveev, B. M. Rassadin, and E. M. Tai, in *Plasma Physics and Controlled Nuclear Fusion Research 1994* (International Atomic Energy Agency, Vienna, 1995), Vol. 1, pp. 749–756.

[16] H. Renner, the WII-AS team, the NBI group, the ICF group, and the ECRH group, Plasma Phys. Controlled Fusion **31**, 1579 (1989).

[17] J. F. Lyon, B. A. Carreras, K. K. Chipley, M. J. Cole, J. H. Harris, T. C. Jernigan, R. L. Johnson, V. E. Lynch, B. E. Nelson, J. A. Rome, J. Sheffield, and P. B. Thompson, Fusion Technol. **8**, 179 (1986).

[18] I. Garcia-Cortes, M. A. Pedrosa, C. Hidalgo, B. Brañas, T. Estrada, R. Balbin, E. de la Luna, J. Sanchez, and A. P. Navarro, Phys. Fluids B **4**, 4007 (1992).

[19] P.-H. Rebut and the JET team, in *Plasma Physics and Controlled Nuclear Fusion Research 1990* (International Atomic Energy Agency, Vienna, 1991), Vol. 1, pp. 27–48.

[20] L. Fellin, P. Kusstatscher, and G. Rostagni, Fusion Eng. Des. **25**, 315 (1995).

[21] C. Riccardi, D. Xuangtong, M. Salierno, L. Gamberale, and M. Fontanesi, Phys. Plasmas **4**, 3749 (1997).

[22] D. R. Cox, in *Statistics: An Appraisal*, edited by H. A. David and H. T. David (The Iowa State University Press, Ames, 1984), pp. 55–74.

[23] G. U. Yule, J. R. Stat. Soc. **108**, 208 (1945).

[24] B. B. Mandelbrot and J. R. Wallis, Water Resour. Res. **5**, 967 (1969).

[25] A. W. Lo, Econometrica **59**, 1279 (1991).

[26] H. E. Schepers, J. H. G. M. van Beek, and J. B. Bassingthwaighte, IEEE Eng. Med. Biol. **11**, 57 (1992).

[27] J. Moody and L. Wu, in *Neural Networks in the Capital Markets*, edited by A. Refenes, Y. Abu-Mostafa, J. Moody, and A. Weigen (World Scientific, London, 1996).

[28] A. Latten, T. Klinger, A. Piel, and T. Pierre, Rev. Sci. Instrum. **66**, 3254 (1995).

[29] T. Klinger, A. Latten, A. Piel, G. Bonhomme, and T. Pierre, Plasma Phys. Controlled Fusion **39**, B145 (1997).

[30] T. Klinger, A. Latten, A. Piel, G. Bonhomme, T. Pierce, and T. Dudola de Wit, Phys. Rev. Lett. **79**, 3913 (1997).

[31] A. A. Tsonis, *Chaos: From Theory to Applications* (Plenum, New York, 1992).

[32] C. Hidalgo, M. A. Pedrosa, B. Ph. van Milligen, E. Sanchez, R. Balbin, I. Garcia-Cortes, J. Bleuel, L. Giannone, and H. Niedermeyer, in *Fusion Energy 1996* (International Atomic Energy Agency, Vienna, 1997), Vol. 1, pp. 617–624.

[33] J. Bleuel, G. Theimer, M. Endler, L. Giannone, H. Niedermeyer, the ASDEX team, and the W7-AS team, in *Controlled Fusion and Plasma Physics* (European Physical Society, Petit-Lancy, 1996), Vol. 20C, pp. 727–730.

[34] C. Hidalgo, J. H. Harris, T. Uckan, J. D. Bell, B. A. Carreras, J. L. Dunlap, G. R. Dyer, C. P. Ritz, A. J. Wootton, M. A. Meier, T. L. Rhodes, and K. Carter, Nucl. Fusion **13**, 1471 (1991).

[35] I. Garcia-Cortes, M. Endler, A. Loarte, S. J. Davis, S. K. Erents, H. Guo, C. Hidalgo, J. Lingertat, J. R. Martin-Solis, G. F. Matthews, B. Ph. van Milligen, R. D. Monk, R. Simonini, and A. Taroni, in *Controlled Fusion and Plasma Physics* (European Physical Society, Berchtesgarden, 1997), Vol. 21A Part 1, pp. 109–112.

Phys. Plasmas, Vol. 5, No. 10, October 1998

Carreras *et al.*   3643

[36] V. Antoni, R. Cavazzana, D. Desideri, E. Martines, G. Serianni, and L. Tramontin, Phys. Rev. Lett. **80**, 4185 (1998).

[37] B. A. Carreras, C. Hidalgo, E. Sanchez, M. A. Pedrosa, R. Balbin, I. Garcia-Cortes, B. Ph. van Milligen, D. E. Newman, and V. E. Lynch, Phys. Plasmas **3**, 2664 (1996).

[38] T. Hwa and M. Kadar, Phys. Rev. A **45**, 7002 (1992).

[39] X. Garbet and R. E. Waltz, Phys. Plasmas **5**, 2836 (1998).

[40] T. L. Rhodes and R. Moyer (private communication, 1997).

[41] D. E. Newman, B. A. Carreras, and P. H. Diamond, Phys. Lett. A **218**, 58 (1996).

[42] C. P. Ritz, H. Lin, T. L. Rhodes, and A. J. Wootton, Phys. Rev. Lett. **65**, 2543 (1990).

[43] K. H. Burrell, Phys. Plasmas **4**, 1499 (1997).

[44] H. Biglari, P. H. Diamond, and P. W. Terry, Phys. Fluids B **2**, 1 (1990).

[45] G. Rewoldt, M. A. Beer, M. S. Chance, T. S. Hahm, Z. Lin, and W. M. Tang, Phys. Plasmas **5**, 1815 (1998).